

A. PUKHOV^{1,✉}
J. MEYER-TER-VEHN²

Laser wake field acceleration: the highly non-linear broken-wave regime

¹ Institut für Theoretische Physik I, Heinrich-Heine-Universität Düsseldorf, 40225 Düsseldorf, Germany

² Max-Planck-Institut für Quantenoptik, Hans-Kopfermann-Str. 1, 85748 Garching, Germany

Received: 12 December 2001

Published online: 14 March 2002 • © Springer-Verlag 2002

ABSTRACT We use three-dimensional particle-in-cell simulations to study laser wake field acceleration (LWFA) at highly relativistic laser intensities. We observe ultra-short electron bunches emerging from laser wake fields driven above the wave-breaking threshold by few-cycle laser pulses shorter than the plasma wavelength. We find a new regime in which the laser wake takes the shape of a solitary plasma cavity. It traps background electrons continuously and accelerates them. We show that 12-J, 33-fs laser pulses may produce bunches of 3×10^{10} electrons with energy sharply peaked around 300 MeV. These electrons emerge as low-emittance beams from plasma layers just 700- μm thick. We also address a regime intermediate between direct laser acceleration and LWFA, when the laser-pulse duration is comparable with the plasma period.

PACS 52.38.Kd; 52.35.-g; 41.75.Ht

1 Introduction

We are evidencing a continuing progress in laser technology, which leads to laser systems delivering ever shorter and more intense pulses. Compact systems generating multi-terawatt (10^{12} W)- and even petawatt (10^{15} W)-range pulses are available now [1]. When focused, the petawatt laser pulses reach intensities up to $I = 10^{21}$ W/cm² and the electric field strength is $E = 10^{14}$ V/m [2]. One of the appealing applications for these lasers is high-gradient laser wake field acceleration (LWFA) of charged particles in plasma [3, 4]. When a laser pulse propagates through underdense plasma, it excites a running plasma wave oscillating with frequency $\omega_p = 4\pi e^2 n_0 / m$, where e , m , and n_0 denote charge, mass, and density of electrons, respectively. The wave trails the laser pulse with phase velocity set by the laser pulse group velocity $v_{\text{ph}}^{\text{wake}} = v_g = c(1 - \omega_p^2 / \omega_0^2)^{1/2}$, where ω_0 is the laser frequency. The electric field of this plasma wave is longitudinal, i.e. it points in the propagation direction. A relativistic electron can ride this plasma wave, staying in-phase with this longitudinal electric field and be accelerated to high energies.

The laser pulse can excite the plasma wave in different ways. The excitation is most effective when the laser pulse is shorter than the plasma wavelength $\lambda_p = 2\pi c / \omega_p$ and fits completely into the first half of the plasma wave. For a pulse with a normalized intensity profile given by $a^2 = a_0^2 \cos^2(\pi\zeta/2L)$ for $-L < \zeta = z - ct < L$, the maximum acceleration field of a plane laser wake field is $E_{\text{max}}/E_0 = a_0^2/(1 + a_0^2)^{1/2}$, when the laser pulse full width at half maximum (FWHM) equals one-half of the plasma period: $L = \lambda_p/2$ [4]. Here, $E_0 = mc\omega_p/e$ normalizes the electric field of the plasma wave, and $a_0 = eA_0/mc^2$ is the normalized amplitude of the laser vector potential. In the present paper, we explore LWFA in the relativistic regime $a_0 > 1$, in which the wake field changes its structure and cannot be described any more by linear plasma theory. The non-linear evolution is followed by three-dimensional particle-in-cell (3D PIC) simulations, and we present numerical results obtained with the code VLPL [5].

The length of the laser pulse is a parameter of particular significance. The pattern of wake field excitation differs significantly for laser pulses longer and shorter than the plasma period. The long laser pulse gets self-modulated with the plasma period, and the resonance between this self-modulation and the plasma frequency leads to effective wake field excitation. The corresponding regime of particle acceleration is called self-modulated laser wake field acceleration (SM-LWFA) [6–9].

Long laser pulses, however, experience not only the one-dimensional self-modulation, but get self-focussed and form relativistic channels in the plasma. Also, several wake field periods stronger than that of the plasma wave by a factor ω_0/ω_p . In this case, the laser field can accelerate electrons directly. This direct laser acceleration (DLA) [10, 11] is very similar to the inverse free-electron laser mechanism and can even dominate over wake field acceleration [12]. In this scheme, electrons gain energy from the transverse electric field of the laser, and the magnetic field turns them in the forward direction.

In the present paper, we focus on laser wake field acceleration in a new, highly non-linear regime. It occurs for laser pulses shorter than λ_p , as described above, but for relativistic intensities high enough to break the plasma wave after the first oscillation. The electric field required for wave breaking

✉ Corresponding author.

Fax: +49-211/811-5194, E-mail: pukhov@thphy.uni-duesseldorf.de

can be estimated from the expression $E_{wb}/E_0 = \sqrt{2(\gamma_p - 1)}$, with $\gamma_p = (1 - v_g^2/c^2)^{-1/2} = \omega_0/\omega_p$ [13], which holds for low-temperature plane plasma waves. In the present relativistic regime, however, one should notice that the plasma wave fronts are curved and first break near the wave axis and for lower values than the plane-wave limit. This has been studied in 2D geometry in [14–17]. Here, we present 3D PIC simulations of two representative cases. The case (I) is just marginally above (see Sect. 2) and the case (II) is far above (see Sect. 3) the breaking threshold.

Wave breaking turns out to be of central importance because it leads to abundant self-trapping of electrons in the potential of the wave bucket, which are then accelerated in large numbers. This results in high conversion efficiency of laser energy into relativistic beam energy; it will be discussed below in the context of Figs. 1, 3 and 4. Trapping of electrons in the plasma waves is a key topic for LWFA. Injection and acceleration of external beams have been demonstrated experimentally [18]. Creation of trapped electrons inside the wave bucket has been proposed with the application of supplementary laser pulses [19, 20]. However, copious amounts of accelerated electrons have been observed when driving waves beyond the breaking threshold; this has been shown in SM-LWFA experiments with single TW laser pulses longer than λ_p [21–25].

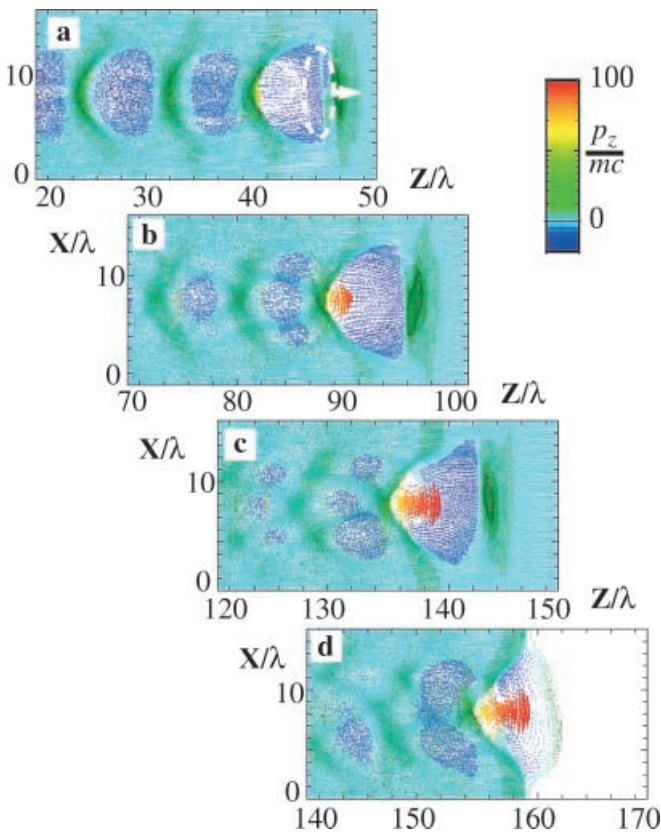


FIGURE 1 Wake field behind a 20-mJ, 6.6-fs laser pulse propagating in a plasma layer from left to right. Cuts along the propagation axis show electron-density evolution of plasma wave (green-blue) and high-energy pulse (orange-red) at times **a** $t = 50 \lambda/c$; **b** $t = 100 \lambda/c$; **c** $t = 150 \lambda/c$; **d** $t = 170 \lambda/c$. Color corresponds to longitudinal electron momentum. The dashed line in frame **a** indicates the position of the laser pulse

A significant difference in the LWFA domain discussed in this paper concerns the energy spectra of the emerging relativistic beams. While most long-pulse experiments have produced energy spectra with exponential fall-off, well characterized by an effective temperature, we find a plateau-like spectrum for case (I) and even a spectrum sharply peaked in energy for the solitary acceleration bubble of case (II). We describe in Sect. 3 how the peaked spectrum is related to beam-loading effects.

In this paper, we can give only numerical results for a few selected cases located in the parameter space spanned by laser intensity and pulse length as well as plasma density. Systematic studies and analytic theory are necessary to connect the various regimes. Nevertheless, we discuss some scaling properties of the new LFWA regime in Sect. 4, based on the short-pulse and the wave-breaking conditions. Posed simultaneously, these two conditions are still a challenge. The scaling shows that few-cycle pulses are best suited. The rapid progress in ultra-short laser technology is expected to produce appropriate pulses very soon. Sub-10-fs laser pulses containing about 1-mJ energy have been demonstrated already [1, 26] and are expected to be upgraded to 10-fs, 10-mJ pulses reaching TW power in the next few years. Lasers producing multi-joule pulses at 30 fs are under construction [27, 28].

In Sect. 5, we have added a third simulation to address the transitional region in which the laser-pulse length is somewhat longer than λ_p and SM-LWFA occurs. This case is discussed in view of recent experiments performed in this regime at Laboratoire d'Optique Appliquée (LOA) [29] and at Michigan University [30]. The experiment made at LOA has produced electrons with energies up to 70 MeV. Based on simulations with test particles injected into the laser wake [29], these results have been explained as a combination of LWFA and DLA. We will show here that our direct VLPL simulations support this explanation.

2 Generation of a sub-10-fs electron bunch

In the simulations, we consider incident laser pulses of the form

$$a(t, r) = a_i \cos(0.5\pi t/\tau_i) \cos(0.5\pi r/\sigma_i), \quad (1)$$

for $-\tau_i < t < \tau_i$ and $r < \sigma_i$. In case (I), we take $\tau_1 = 6.6$ fs, $a_1 = 1.7$, $\sigma_1 = 5\lambda$, $\lambda = 1 \mu\text{m}$, and energy $W_1 = 20$ mJ. The laser pulse is circularly polarized and propagates through a uniform plasma with electron density $n_e = 3.5 \times 10^{19} \text{ cm}^{-3}$. Figure 1 shows four movie frames, following the front of the plasma wave as it propagates in the z direction. The laser pulse is indicated only in the first frame by the broken line behind the wave front. The frames show electron density in cuts along the laser-beam propagation axis. Each dot corresponds to one numerical electron and is colored according to its momentum p_z/mc . This way of plotting brings out both the structure of the plasma wave and the self-trapped electrons accelerated to high energies in the first wave bucket. Figure 1a shows the wave when it has propagated 45 laser wavelengths into the layer. Like a snow-plough, the laser pulse pushes the front layer of compressed few-MeV electrons (dark green) and leaves a region with low electron density behind. It still con-

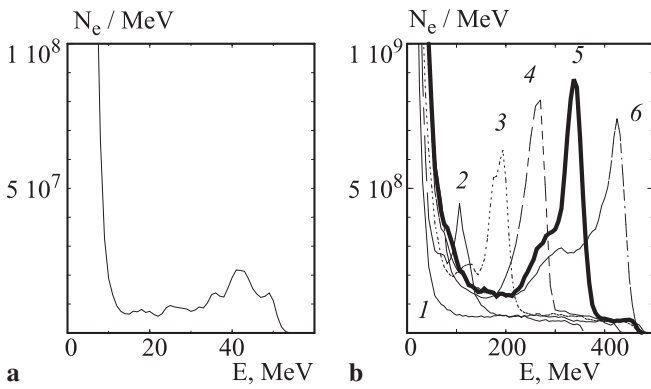


FIGURE 2 Spectra of accelerated electrons: **a** final spectrum of the case of Fig. 1; **b** the case of the 33-fs, 12-J laser pulse, time evolution of the energy spectrum: (1) $ct/\lambda = 350$, (2) $ct/\lambda = 450$, (3) $ct/\lambda = 550$, (4) $ct/\lambda = 650$, (5) $ct/\lambda = 750$ corresponding to Figs. 3, 4, and 5, (6) $ct/\lambda = 850$

tains a population of blue electrons, which stream from right to left and feed the wave structure trailing the pulse.

The green wave crests are curved and start to break at their vertex near the propagation axis. The curvature reflects the 3D structure of a plasma wave with transverse size of order λ_p . A study in 2D geometry [15] has shown that these curved wavefronts break at considerably lower wave amplitudes than plane fronts. In the present 3D simulation, wave breaking occurs already for $E_{\max}/E_{wb} \approx 0.3$ and strong electron depletion is observed only in the first wave bucket. When comparing with non-broken wake fields, the conspicuous new feature in Fig. 1b–d is the stem of relativistic electrons growing out of the base with a cross section of $\sigma_{tr} \approx 0.3 \mu\text{m}^2$ in this case. The energy rises toward the top of the stem, with red electrons which have been trapped first and accelerated over the full propagation distance. This cavity with a stem is a surprisingly stable structure. It is hardly affected by the drop in laser intensity, which decreases steadily due to energy transfer to electrons. The efficiency of electron acceleration in the cavity is surprisingly high. At the end about 15% of the initial laser energy has been transferred to the electron bunch. In Fig. 1d the cavity arrives at the rear boundary of the plasma layer and bursts, releasing the relativistic electron load into vacuum.

The electron pulse produced here consists of about 10^9 relativistic electrons in the range $10 < \gamma < 100$, compressed to a density above the ambient electron density and a pulse length of just 5 fs. The energy spectrum consists of a plateau extending from 1 to 50 MeV, as is seen in Fig. 2a. The spectrum is clearly non-thermal and thus different from the energy spectra observed with long laser pulses. Emerging from a 2- μm spot with an angular divergence of about $\pm 1^\circ$, the electron bunch has a normalized emittance of $\gamma\epsilon_\perp < \pi \text{ mm mrad}$, better than existing electron sources. These pulses may have a broad range of applications, in particular for ultra-short, ultra-bright, high-repetition-rate sources of X-rays and nuclear radiation (positrons, neutrons, etc.).

3 Quasi-monoenergetic beams of electrons from laser-plasma cavities

As the second example (case II), we present the simulation of a laser pulse with $a_2 = 10$, $\tau_2 = 33 \text{ fs}$, and $\sigma_2 =$

12λ , propagating in plasma with $n_e = 10^{19} \text{ cm}^{-3}$. A 3D perspective view of the fast electrons at time $ct/\lambda = 700$ is given in Fig. 3. Here we plot each 100th electron above 10 MeV as a dot colored according to its energy. We see that the highly compressed stem of energetic electrons has a uniform color, corresponding to a peak in the spectrum. The evolution of this peak will be discussed in more detail below.

The wake field in this high-intensity regime is different from that in Fig. 1. As seen in Fig. 4a–c, it has mutated into a solitary cavity, and wave breaking has washed out all downstream structure. The laser pulse is so strong that it scatters electrons sideways, leaving an empty cavity behind. Comparing Fig. 4a and b, we see that the cavity stretches and the stem elongates with time. At $ct/\lambda = 700$ the stem contains

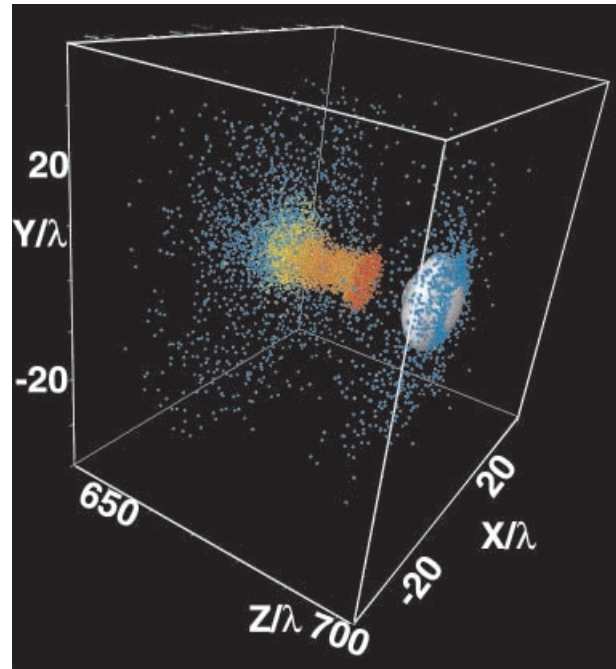


FIGURE 3 The case of a 12-J, 33-fs laser pulse after propagating $z/\lambda = 690$ in 10^{19} cm^{-3} plasma. 3D perspective view of hot electron distribution. Each 100th electron above 10 MeV is shown as a dot colored according to its energy. The white disc shows the laser-intensity surface at $I = 10^{19} \text{ W/cm}^2$

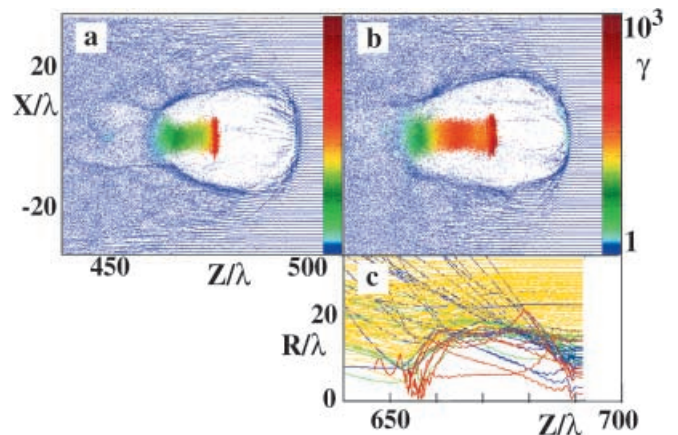


FIGURE 4 Solitary laser-plasma cavity produced by 12-J, 33-fs laser pulse. **a** $ct/\lambda = 500$, **b** $ct/\lambda = 700$, **c** electron trajectories in the frame moving together with the laser pulse; color distinguishes electron groups with different distances from the axis initially

about 3.5×10^{10} electrons with energy 300 ± 30 MeV. They have an angular spread of $\pm 2^\circ$ and represent a genuine beam of 1.8-J full energy. This amounts to 15% of the incident laser energy.

Figure 4c displays selected electron trajectories in a simulation window co-moving with the laser pulse. Electrons far from the propagation axis have yellow trajectories and are hardly perturbed by the pulse. Blue and green electrons, hit by outer regions of the pulse, are scattered outwards. We see how the pulse scatters electrons aside directly and the electron motion becomes multi-stream already at the pulse head. These scattered electrons never return to the cavity region. The red electrons feeding the stem originate close to the axis, and the laser pulse could not scatter them far away. Most of the laser-excited electrons move in half-circles wrapping the cavity. Their trajectories cross each other at the rear vertex, and some get trapped. We find the trapping cross-section to be $\sigma_{tr} \approx 3 \mu\text{m}^2$ for these parameters.

On-axis distributions of key quantities are shown in Fig. 5a–d at $ct/\lambda = 700$. The laser intensity, Fig. 5a, initially 10-cycles long, underwent self-modulation and developed a steep front with a peak intensity much larger than the incident one. This is due to group-velocity dispersion, causing high-intensity parts to travel faster and to form an optical shock [31, 32]. It compresses electrons in front of it into a layer with 20 times the unperturbed plasma density n_0 , see Fig. 5b. Between this layer and the stem electrons, there is a void. The longitudinal electric field, Fig. 5c, jumps sharply at the compressed cavity front and then falls smoothly inside the cavity. The relativistic stem is also highly compressed, up to $18n_0$. Yet, the corresponding space charge causes no jump in the longitudinal electric field E_z . This is due to the $1/\gamma^2$ reduction of E_z for relativistically moving charges [33]. The transverse field, however, is large and only partially compensated by the pinching effect of the magnetic field of the stem. This radial E -field delays background electrons to flow in ra-

dially and to close the cavity. Apparently, beam loading of the cavity occurs by radial inflow of electrons. Longitudinal beam loading of plasma waves has been observed earlier in 2D PIC simulations [14]. In the present 3D simulation, the beam loading is transverse.

The growth of the stem and the evolution of its spectrum are continuous. This is shown in Fig. 2b. At time $ct/\lambda = 350$, the high-energy branch of the spectrum corresponding to the stem has still the plateau structure observed also in the previous case (I) of Fig. 2a. The electrons forming the head of the stem preserve this feature and are seen in the spatially resolved spectrum of Fig. 5d as the cutting-edge in the tomahawk-like distribution. However, the spectra shown in Fig. 2b change at time $ct/\lambda = 450$ and develop a distinct peak which grows in time. This peak starts to appear when the total charge of the stem becomes equal to the charge expelled from the cavity by the driving laser pulse. Then the cavity elongates, and this has the consequence that the front and the rear sides of the cavity move at different speeds. The foot point at which the stem is fed by fresh electrons then lags behind, and this produces the spectral feature seen as the tomahawk handle in Fig. 5d. Clearly, there is an accumulation of electrons with $\gamma \approx 600$, which explains the peak in the z -integrated spectrum. The formation of this energy peak is described here for the first time and represents an important result of this work.

4 Scaling laws

So far, we have presented two numerical examples of electron trapping and acceleration in the broken-wave regime of LWFA. For the 6.6-fs laser pulse, we needed only 20-mJ energy to reach this regime. However, the 30-fs-long laser pulse already required 12 J. The laser energy necessary to reach the solitary cavity regime strongly increases with pulse duration. The pulse duration or, equivalently, the number of laser cycles N determines all other laser parameters and the plasma density.

Here we provide simple scalings with N , based on analytic relations of linear plasma theory [3, 4]. The first requirement is that the laser pulse is shorter than the plasma wavelength, and this leads to $N \propto \omega_0/\omega_p \propto n_0^{-1/2}$. Increasing pulse length implies lower plasma density. The second requirement is to break the wake field. Setting $E_{\text{max}}/E_{\text{wb}} = \text{const.}$, we find that the laser intensity $I\lambda^2 \propto a_0^2 \propto \omega_0/\omega_p \propto N$ scales linearly with pulse duration. Furthermore, the diameter of the laser focus should also be of the order of λ_p to insure a sufficiently plane wake field in the cavity. This requires a laser pulse with power $\propto N^3$ and energy $\propto N^4$. We conclude that few-cycle laser pulses are best suited to reach the new regime. Of course, the energy of the accelerated electrons also depends on N and demands 15–20 cycles to reach the GeV level. The maximum electron energy scales like $W_{\text{max}} = eE_{\text{max}}L_d \propto a_0(\omega_0/\omega_p)^2 \propto N^{5/2}$. Here, $L_d \simeq \gamma_p^2\lambda_p$ is the detuning length [4], which measures the distance over which an electron is accelerated, before it outruns the wave and gains no more energy. It should be emphasized that these scaling arguments can serve only as a very rough guideline and need to be substantiated by 3D simulation in each particular case. These simulations demand large computer resources and easily hit the limits of present-day parallel machines.

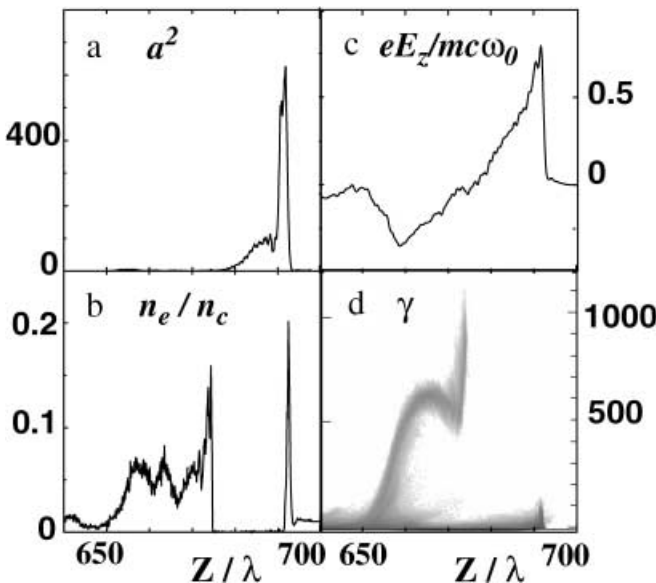


FIGURE 5 Same case as in Figs. 3 and 4 at time $ct/\lambda = 700$. On-axis distributions of **a** laser intensity; **b** electron density; **c** longitudinal electric field; and **d** projection of the electron phase space γ vs z

5 Transition from DLA to LWFA regimes

In the simulations presented here, we have observed electron acceleration by the pure LWFA mechanism. We know, however, that another acceleration mechanism, DLA [10, 12], works at higher plasma densities and longer laser pulses. It is of interest also to give an example for the transitional regime, when both mechanisms DLA and (SM-)LWFA co-exist. Our main goal here is to demonstrate that this regime differs significantly from pure LWFA in the way electrons gain energy.

For this purpose, we have performed a third simulation (case III). The incident laser pulse used in the simulation has here a Gaussian form $a = a_3 \exp(-(t/\tau_3)^2) \exp(-(r/\sigma_3)^2)$, with $a_3 = 1.2$, $\tau_3 = 24$ fs, and $n_e = 0.06n_c$, so that the laser pulse FWHM ≈ 30 fs is 2.5 times longer than the plasma period. The focal spot was $\sigma_3 = 10\lambda$, $\lambda = 0.8 \mu\text{m}$. These values are close to those of experiments performed recently at Michigan [30] and LOA [28]. In the simulation, the laser pulse was propagating through a slab of gaseous N_2 with molecular density $n_m = 1 \times 10^{19} \text{ cm}^{-3}$ as in [30]. In the VLPL code, ionization is treated as field ionization by barrier suppression. The laser pulse is intense enough to ionize nitrogen atoms five times. This leads to the background electron density of $n_e = 1 \times 10^{20} \text{ cm}^{-3}$ in the plasma channel, or $n_e = 0.06n_c$.

Distributions of laser intensity and electron density after propagating $200 \mu\text{m}$ into the plasma are shown in Fig. 6a and b. We see in Fig. 6a that the laser pulse has undergone self-modulation, Raman scattering, and relativistic filamentation simultaneously. It did generate a strong wake field as seen in the electron-density plot, Fig. 6b, and one also observes fast electrons, trapped in the first wake and seen as a black spot at its rear side on the axis. The electron-energy spectrum is shown in Fig. 7a. The spectrum has an exponential slope with an effective temperature of about 3 MeV and a cut-off at 35 MeV. It contains altogether a few 10^9 electrons above 1 MeV. The angular distribution is given in Fig. 7b, showing an angular spread of $\pm 2^\circ$ at half-maximum. The energies and electron numbers obtained here are significantly larger than in [30], but compare reasonably well with the results of [28].

The main interest in this section is to understand the mechanism of electron acceleration. The particle-in-cell simulations allow us to split the energy gain of each electron into components obtained from longitudinal and transverse electric fields, respectively. Analysis in [12] had revealed that electron beams generated by long (much longer than the plasma wavelength) laser pulses in self-focussed plasma channels received most of their energy directly from the transverse laser field. Here, we apply this analysis to case III and compare with case I. The corresponding results are presented in Fig. 7c and d. While case I in Fig. 7c is a clear demonstration of the pure longitudinal LWFA acceleration, case III in Fig. 7d is transitional, where DLA and LWFA are mixed. We mention that Fig. 7d is very similar to the one obtained by Malka et al. [29] for similar parameters [28]. This mixed acceleration originates from the fact that the trapped electrons in case III are located in the region of the self-focussed laser pulse (compare Fig. 6a and b) and therefore experience both the laser field and the wake field.

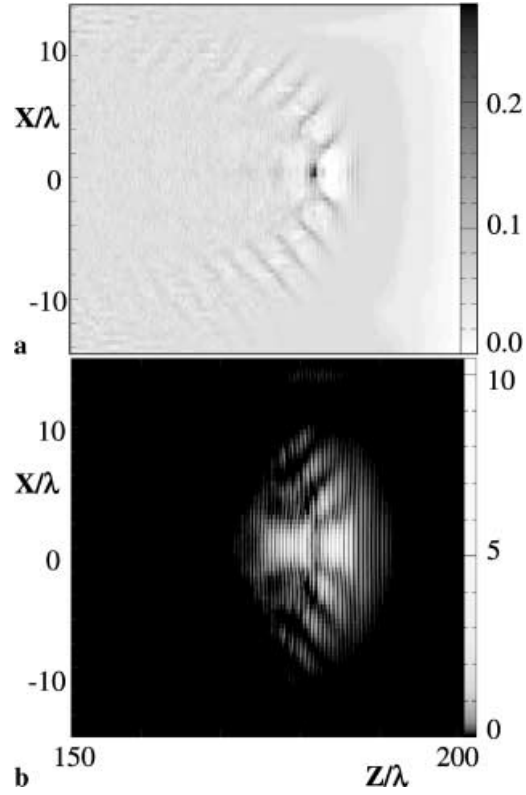


FIGURE 6 Distributions of **a** electron density and **b** intensity for a 0.6-J laser pulse propagating in a N_2 -gas slab of molecular density $n_m = 1 \times 10^{19} \text{ cm}^{-3}$

In our analysis we make use of the equation $dp^2/dt = -2e\mathbf{E} \cdot \mathbf{p} = -2eE_z p_z - 2e\mathbf{E}_\perp \cdot \mathbf{p}_\perp$, stating that energy gain is only due to the electric field and can be divided into a longitudinal and a transverse component. For each numerical electron, we integrate over time from 0 to t to obtain the gain components

$$\Gamma_z = - \int_0^t \frac{2eE_z p_z}{(mc)^2}, \quad \Gamma_\perp = - \int_0^t \frac{\mathbf{E}_\perp \cdot \mathbf{p}_\perp}{(mc)^2}. \quad (2)$$

In Fig. 7c and d, each electron is plotted in the gain plane spanned by Γ_z and Γ_\perp . Note that the relativistic γ -factor of each electron has to satisfy $\gamma^2 = 1 + (p/mc)^2 = 1 + \Gamma_z + \Gamma_\perp > 0$, and therefore all electrons are located in the upper-right half-plane.

For case I, shown in Fig. 7d and corresponding to Fig. 1, electrons have apparently gained energy by the longitudinal wake field alone and satisfy $\Gamma_z \gg |\Gamma_\perp|$. This is in marked contrast to Fig. 7c obtained for case III in which the accelerated electrons have experienced both the wake field E_z and the laser field E_\perp and occupy a broad region of the Γ_z, Γ_\perp plane. The white dashed lines enclose areas preferably populated by DLA and LWFA, respectively. Notice that DLA leads to large values of Γ_\perp and negative (!) Γ_z , indicating deceleration by the longitudinal E_z -field. This is attributed to the laser field, which has large E_\perp and simultaneously a negative E_z component when propagating in a narrow channel. One should also realize that, notwithstanding transverse acceleration, electrons move predominantly in the laser direction

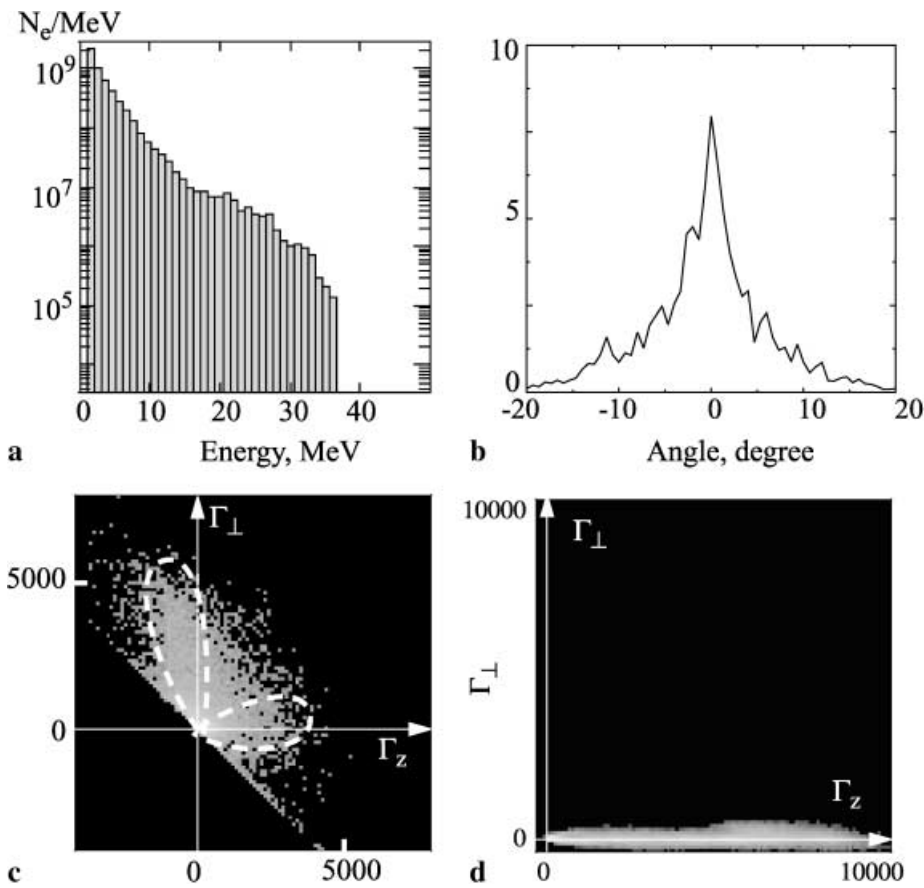


FIGURE 7 **a** Electron spectrum, **b** angular distribution, and **c** energy-gain plane (Γ_z , Γ_\perp) for the case of Fig. 6; the *dashed white lines* indicate the populations arising from DLA (large Γ_\perp) and (SM-)LWFA (large Γ_z). **d** For comparison, electron distribution in (Γ_z , Γ_\perp) plane for pure LWFA case of Fig. 1

forming the relativistic beam; the longitudinal motion is due to $\mathbf{v} \times \mathbf{B}$ forces which push the electrons in the z direction without energy transfer.

Finally, we mention that Malka et al. [29] have used $\mathbf{E} \cdot \mathbf{v}$ rather than $\mathbf{E} \cdot \mathbf{p}$ in (2) to calculate the electron energy instead of its square. The differencing scheme used in VLPL, however, allows us to calculate $\mathbf{E} \cdot \mathbf{p}$ more directly without additional interpolation. For reasons of numerical accuracy, we have therefore preferred this second option in the present work.

6 Conclusions

In this work we have considered the wake field acceleration of electrons in the broken-wave regime. This kinetic and highly non-linear regime is difficult to treat analytically, and therefore we have studied it numerically. We find that the 3D wave breaking of the laser wake field can produce electron bunches with unique properties. A sub-10-fs laser pulse with only 20-mJ energy is able to accelerate 10^9 electrons with a flat spectrum reaching 50-MeV energy. A spectrum sharply peaked in energy is obtained for a 12-J, 30-fs laser pulse. In this case the laser is intense enough to expel all background electrons from the first wake trough, forming a solitary cavity and a completely broken wake field further downstream. Propagating through plasma, this cavity continuously traps a small portion of background electrons and generates an almost mono-energetic beam of 3×10^{10} electrons at 300 MeV.

These new results call for experimental verification. At present we have to rely on our 3D PIC simulations. However, we recall that PIC simulations have been very successful in reproducing existing experiments [12, 14, 34]. The fast development of laser technology suggests that the laser pulses with corresponding parameters will be available in the near future.

ACKNOWLEDGEMENTS The work was supported in part by the Alexander von Humboldt Foundation in the framework of the Sofja Kovalevskaja Program, and also by BMBF and DFG, Bonn. The VLPL code was run on a CRAY-T3E at Rechenzentrum Garching.

REFERENCES

- 1 G. Mourou, C. Barty, M. Perry: *Physics Today*, Jan. (1998), p. 22
- 2 M.H. Key, M.D. Cable, T.E. Cowan, K.G. Estabrook, B.A. Hammel, S.P. Hatchett, E.A. Henry, D.E. Hinkel, J.D. Kilkenny, J.A. Koch, W.L. Krueer, A.B. Langdon, B.F. Lasinski, R.W. Lee, B.J. MacGowan, A. MacKinnon, J.D. Moody, M.J. Moran, A.A. Offenberger, D.M. Pennington, M.D. Perry, T.J. Phillips, T.C. Sangster, M.S. Singh, M.A. Stoyer, M. Tabak, G.L. Tietbohl, M. Tsukamoto, K. Wharton, S.C. Wilks: *Phys. Plasmas*, **5**, 1966 (1998)
- 3 T. Tajima, J. Dawson: *Phys. Rev. Lett.* **43**, 267 (1979)
- 4 E. Esarey, P. Sprangle, J. Krall, A. Ting: *IEEE Trans. Plas. Sci.* **24**, 252 (1996)
- 5 A. Pukhov: *J. Plasma Phys.* **61**, 425 (1999)
- 6 P. Sprangle, E. Esarey, J. Krall: *Phys. Rev. Lett.*, **69**, 2200 (1992)
- 7 N.E. Andreev, L.M. Gorbunov, V.I. Kirsanov, A.A. Pogosova, R.R. Ramayashvili: *JETP Lett.*, **55**, 571 (1992)
- 8 T.M. Antonsen, P. Mora: *Phys. Rev. Lett.*, **69**, 2204 (1992)
- 9 E. Esarey, J. Krall, P. Sprangle: *Phys. Rev. Lett.*, **72**, 2887 (1994)
- 10 A. Pukhov, Z.M. Sheng, J. Meyer-ter-Vehn: *Phys. Plasmas*, **6**, 2847 (1999)

- 11 A. Pukhov, J. Meyer-ter-Vehn: Phys. Rev. Lett. **76**, 3975 (1996)
- 12 C. Gahn, G.D. Tsakiris, A. Pukhov, J. Meyer-ter-Vehn, G. Pretzler, P. Thirof, D. Habs, K.J. Witte: Phys. Rev. Lett. **83**, 4772 (1999)
- 13 A.I. Akhiezer, R.V. Polovin: JETP **3**, 696 (1956)
- 14 K.-C. Tzeng, W.B. Mori, T. Katsouleas: Phys. Plasmas **6**, 2105 (1999)
- 15 S.V. Bulanov, F. Pegoraro, A. Pukhov, A.S. Sakharov: Phys. Rev. Lett. **78**, 4205, (1997)
- 16 T.V. Liseikina, F. Califano, V.A. Vshivkov, F. Pegoraro, S.V. Bulanov: Phys. Rev. E **60**, 5991 (1999)
- 17 J.K. Kim, D. Umstadter: In: Advanced Accelerator Concepts: 8th Workshop. AIP Conf. Proc. **472** (AIP Press, N.Y. 1999), p. 404
- 18 F. Amiranoff, D. Bernard, B. Cros, F. Dorchie, F. Jacquet, V. Malka, J.R. Marques, G. Matthieussent, P. Mine, A. Modena, J. Morillo, Z. Najmudin: Nucl. Instr. and Methods in Phys. Res. **410A**, 364 (1998)
- 19 E. Esarey, R.F. Hubbard, W.P. Leemans, A. Ting, P. Sprangle: Phys. Rev. Lett. **79**, 2682 (1997)
- 20 D. Umstadter, J.K. Kim, E. Dodd: Phys. Rev. Lett. **76**, 2073 (1996)
- 21 A. Modena, Z. Najmudin, A.E. Dangor, C.E. Clayton, K.A. Marsh, C. Joshi, V. Malka, C.B. Darrow, C. Danson, D. Neely, F.N. Walsh: Nature (London) **337**, 606 (1995)
- 22 S.-Y. Chen, M. Krishnan, A. Maksimchuk, R. Wagner, D. Umstadter: Phys. Plasmas **6**, 4739 (1999)
- 23 A. Ting, K. Krushelnick, C.I. Moore, H.R. Burris, E. Esarey, J. Krall, P. Sprangle: Phys. Rev. Lett. **77**, 5377 (1996)
- 24 D. Gordon, K.C. Tzeng, C.E. Clayton, A.E. Dangor, V. Malka, K.A. Marsh, A. Modena, W.B. Mori, P. Muggli, Z. Najmudin, D. Neely, C. Danson, C. Joshi: Phys. Rev. Lett. **80**, 2133 (1998)
- 25 M. Santala, Z. Najmudin, E.L. Clark, M. Tatarakis, K. Krushelnick, A.E. Dangor, V. Malka, J. Faure, R. Allott, R.J. Clarke: Phys. Rev. Lett. **86**, 1227 (2001)
- 26 F. Krausz: private communication; S. Sartania, Z. Cheng, M. Lenzer: Opt. Lett. **22**, 1562 (1997)
- 27 I.N. Ross: Opt. Commun. **144**, 125 (1997)
- 28 A. Antonetti, F. Blasco, J.P. Chambaret, G. Cheriaux, G. Darpentigny, C. LeBlanc, P. Rousseau, S. Ranc, G. Rey, F. Salin: Appl. Phys. B **65**, 197 (1997)
- 29 V. Malka, J. Faure, J.R. Marques, F. Amiranoff, J.P. Rousseau, S. Ranc, J.P. Chambaret, Z. Najmudin, B. Walton, P. Mora, A. Solodov: Phys. Plasmas **8**, 2605 (2001)
- 30 X. Wang, M. Krishnan, N. Saleh, H. Wang, D. Umstadter: Phys. Rev. Lett. **84**, 5324 (2000)
- 31 C.E. Max: Phys. Rev. Lett. **33**, 209 (1974)
- 32 C. Ren, B.J. Duda, R.G. Hemker, W.B. Mori, T. Katsouleas, T.M. Antonen, Jr., P. Mora: Phys. Rev. E **63**, 026411-1 (2001)
- 33 J.D. Jackson: *Classical Electrodynamics*, 3rd edition (J. Wiley & Sons Inc. 1999), p. 561
- 34 H. Ruhl, Y. Sentoku, K. Mima, K.A. Tanaka, R. Kodama: Phys. Rev. Lett. **82**, 743 (1999)